Materials Today Bio 16 (2022) 100422

Contents lists available at ScienceDirect

Materials Today Bio

journal homepage: www.journals.elsevier.com/materials-today-bio

# Injectable demineralized bone matrix particles and their hydrogel bone grafts loaded with β-tricalcium phosphate powder and granules: A comparative study

Hoe-Jin Kang [a], Seong-Su Park [b], Garima Tripathi [a], Byong-Taek Lee [a,b,*]

[a] Institute of Tissue Regeneration, College of Medicine, Soonchunhyang University, Cheonan, South Korea
[b] Department of Regenerative Medicine, College of Medicine, Soonchunhyang University, Cheonan, South Korea

ARTICLE INFO

*Keywords:*
Demineralized bone matrix
β-Tricalcium phosphate
Injectable bone substitute

ABSTRACT

Demineralized bone matrix (DBM), has been used as a bone-graft material because of its osteoconductivity and osteoinductivity. However, the previous research report that supports the single use of DBM is limited by its rapid resorption caused by the lack of calcium and phosphate. β-Tricalcium phosphate (TCP) is an enriched calcium phosphate material suitable for bone healing with osteoconductive properties. In this study, we have developed injectable bone graft by the loading two kinds of TCP in DBM particles and thermo-sensitive DBM-derived hydrogel (hDBM). TCP powder (pTCP) and TCP granules (gTCP) were loaded into hDBM and DBM, respectively. The bone formation effect was investigated according to the morphological features of TCP. Residual growth factor concentrations were investigated; microstructure and morphology were characterized by SEM. *In-vitro* studies showed that hDBM/DBM/pTCP and hDBM/DBM/gTCP bone grafts were biocompatible and could promote osteogenesis by up-regulating the expression of Runx2 and OPN, bone-related genes. *In-vivo* studies using the rabbit-femur defect model revealed that the implanted hDBM/DBM/pTCP bone graft showed similar histology to that of fibrous dysplasia with the expression of CD68, whereas hDBM/DBM/gTCP showed good bone formation. Loading of gTCP in place of pTCP was noticed as an effective way to improve bone regeneration in an injectable hDBM/DBM hydrogel-based bone graft.

## 1. Introduction

Demineralized bone matrix (DBM) is widely used for bone regeneration because of its osteoconductivity and osteoinductivity. DBM can provide some structural support and biochemical advantages to cells for effective tissue remodeling. Furthermore, extracellular matrix (ECM) proteins, collagen I, and several growth factors (vascular endothelial growth factor, VEGF; transforming growth factor β1, TGF-β1; bone morphogenic proteins, BMPs; and others) are found in the DBM; these augment osteogenic differentiation and vascularization, as well as induce bone formation and remodeling [1–3].

For application in bone defects, DBM-derived hydrogel (hDBM) is being used as a carrier for TCP or other growth factors [4–6]. A tissue-engineered hydrogel, fabricated from DBM (and consequently ECM), mimics key attributes of the intrinsic tissue microenvironment which motivates the delivery of structural support as well as endogenous bioactive signals [5,7–9]. Macromolecular components of DBM can be released spatiotemporally from biological hydrogel as matricryptins (such as growth factors, small ECM fragments, and peptides), which stimulate cell-cell and cell-matrix communication, tissue regeneration, and remodeling [10,11]. Recent studies have shown that native tissue-derived decellularized bone hydrogels can be used for tissue healing [12]. Further, DBM hydrogels incorporated with growth factors which demonstrated improved mineralization and skeletal tissue regeneration in chick femur defects [13]. In spite of several advantages, the restricted use of DBM is inefficient for clinical application due to tissue collapse after implantation [14,15]. DBM only cannot fulfill the role of sufficient scaffold owing to lack of calcium/phosphate and causing rapid resorption before new bone formation occurs.

Therefore, in order to improve DBM's ability for bone-graft material, mixing DBM with calcium phosphate enriched material may be a key. One of the most commonly used forms of calcium phosphate for synthetic bones is β-tricalcium phosphate (TCP), which has been widely studied in the field of tissue regeneration as a result of its osteoconductivity,

* Corresponding author. Institute of Tissue Regeneration, College of Medicine, Soonchunhyang University, Cheonan, South Korea.
*E-mail address:* lbt@sch.ac.kr (B.-T. Lee).

https://doi.org/10.1016/j.mtbio.2022.100422
Received 19 June 2022; Received in revised form 6 September 2022; Accepted 7 September 2022
Available online 9 September 2022

biocompatibility, and bio-resorption [16,17]. In particular, since TCP has a suitable rate of degradation, it can promote the release of calcium and phosphorus ions to induce bone formation [18].

In this work, we obtained porcine-derived DBM particles by means of demineralization and decellularization. Thermo-sensitive DBM-derived hydrogel (hDBM) is prepared to use as an easy-to-apply for bone grafting. Also, to improve DBM's capability as a bone graft, it was further modified with TCP into the hDBM/DBM.

Two different types of TCP (TCP powder, pTCP; TCP granules, gTCP) were mixed with hDBM/DBM respectively. Micron-sized pTCP can be expected to provide calcium phosphate ions easily and uniformly. Cylindrical gTCP granules with a diameter of 1 mm and a length of 1 mm have 7 interconnected channels [18]. gTCP can promote cell migration through the porous structure, and it can be expected to serve as a sufficient scaffold for the defect site. We examined the bone formation behavior according to the TCP structural morphology by mixing different types of TCP with hDBM/DBM.

We have investigated the microstructure, cytocompatibility, and osteogenic differentiation ability of hDBM, hDBM/DBM, hDBM/DBM/pTCP, and hDBM/DBM/gTCP bone grafts. Also, comparative bone regeneration properties based on different TCP morphology with hDBM/DBM were evaluated by *in-vivo* performance in a rabbit femoral-defect model for 1 and 2 months.

## 2. Materials and methods

### 2.1. Preparation of porcine bone

Fresh porcine femurs were purchased from a local livestock market (Cheonan, Korea) and were chopped for further use. The bone was cleaned and washed with phosphate-buffered saline (PBS) containing 0.1% Gentamicin (Gibco, US). Washed bones were frozen by liquid nitrogen and then ground to ~4 $mm^3$ or less, by a commercial grinder (Han-Il, Korea).

### 2.2. Demineralization and decellularization of bone matrix

Demineralized bone matrix (DBM) was processed by previously described protocols [19]. Ground porcine bone matrix was demineralized under continuous stirring @ 300 rpm in 0.5 N HCl (25 ml per 1g of bone) (DukSan, Korea) at room temperature, for 24 h. After demineralization, the bone matrix was rinsed three times with distilled (DI) water for 20 min. Then, the lipid in DBM was removed with a 1:1 mixture of methanol and chloroform for 1hr. The DBM was snap frozen at −80 °C, lyophilized for 24 h, and stored at −20 °C until required.

For decellularization of DBM, the lyophilized-demineralized bone matrix was rinsed with DI water and added into a 0.05% trypsin and 0.02% EDTA solution at 37 °C for 24 h (Sigma, US). Then bone matrix was rinsed in PBS supplemented with 1% w/v penicillin/streptomycin (Sigma, US) on a stir plate at 4 °C for 24 h. The decellularized bone matrix was snap frozen at −80 °C, lyophilized for 24 h, and stored at −20 °C until required.

### 2.3. Confirmation of DNA contents

DBM was verified by histological analysis and DNA quantification. For histological analysis, native bone matrix (NBM) and DBM were fixed with 4% paraformaldehyde (PFA) and dehydrated prior to embedding in paraffin. NBM and DBM in the paraffin-embedded blocks were sectioned at 5 μm thickness by microtome (Thermo-Scientific, USA). The sections of NBM and DBM were stained with hematoxylin and eosin (H & E) to confirm the removal of cellular contents after decellularization.

For DNA quantification, the total DNA of NBM and DBM were extracted and quantified it using a DNA Quantification Kit (GeneAll, 104–101, Korea). The extracted DNA from NBM/DBM was run in 1% agarose gel with a DNA ladder (Biorad, US).

### 2.4. Preparation of DBM-derived thermo-sensitive hydrogel

To digest DBM, lyophilized DBM was added to 1 mg/ml pepsin (Sigma, US) in 0.01 N HCl for a concentration of 20 mg bone matrix per ml. The suspension was mixed on a stir plate at room temperature for 96 h, until no visible bone matrix remained. To prepare the 10 mg/ml DBM hydrogel (hDBM), 50 ml of digested DBM, 10 ml of 10x PBS, 5 ml of 0.1 N NaOH, and 35 ml of DI water were mixed together and stored at 4 °C until required.

### 2.5. Quantification of growth factors

Protein contents in DBM and hDBM were evaluated by quantifying growth factors with NBM as the control. Concentrations of growth factors in the DBM and hDBM were quantified using a Quantikine ELISA Kit. The concentrations of bone morphogenetic protein-2 (BMP-2, R&D Systems, DBP200, US), transforming growth factor-β1 (TGF-β1, R&D Systems, DB100C, US), and vascular endothelial growth factor (VEGF, R&D Systems, DVE00, US)) were evaluated. For the quantification of the growth factors, the ELISA kit required a pre-treated bone matrix immersed in 1 N HCl. The ELISA kits were performed according to the instructions of the manufacturer.

### 2.6. Characterization of DBM hydrogel

The gelation of injectable hDBM was confirmed by a tube inversion test. Briefly, the injectable hDBM was transferred into a microcentrifuge tube and exposed to a water bath with a temperature of 37 °C. The sol-gel transition of injectable hDBM was determined by inverting the tubes. Sol is defined as a free-flowing liquid while gel is a non-flowing solid gel.

Turbidimetric gelation of the hDBM was evaluated as previously reported [19]. Briefly, 100 μl of hDBM was kept at 4 °C and transferred to 96-well plates. The plates were incubated at 37 °C and the absorbance of the samples was read at 405 nm using a microplate reader (Bio-Tek, Korea). Turbidimetric gelation of the hDBM was monitored every 2 min for 40 min. The normalized values were calculated using Equation (1), where N.A is the normalized absorbance, $A$ is the absorbance at a given time, $A_0$ is the initial absorbance, and $A_{max}$ is the maximum absorbance of the sample. And then used to calculate the following kinetic parameters: The Lag time ($T_{Lag}$) was defined as the intercept of the linear region of the gelation curve with 0% absorbance, the Time to half gelation ($T_{1/2}$) as the time to 50% absorbance, the Time to complete gelation ($T_1$) as the time to 100% absorbance.

$$N.A = \frac{(A - A0)}{(Amax - A0)} \quad (1)$$

Viscosity and shear modulus of hDBM at 37 °C were determined using a Brookfield Viscometer (Model RV, Brookfield, Middleboro, MA, USA) with an SC4—12RPY sample adapter and an SC4-27 spindle. The viscosity was determined at an increasing shear rate.

### 2.7. Preparation of β-tricalcium phosphate granules

TCP powders (pTCP) were procured from Inobone Co., Ltd. (Cheonan, Korea). The particle size of TCP powder is 0.5~1 μm. TCP granules (gTCP) were prepared by a multi-pass extrusion method as described previously [18]. The gTCP is cylindrical seven interconnected multichannel granule, of 1 mm (d) X 1 mm (h). In order to form these multichannel granules channels, carbon powder (Sigma, US) was employed as a pore former in the process. To prepare cylindrical TCP scaffolds, TCP and carbon powder were separately combined with a binder (ethylene vinyl acetate, EVA; Dupont, US) and a lubricant (stearic acid; Daejung, Korea) using a shear mixer (C.W. Brabender Instruments, Korea). The mixture was then shaped by warm pressing prior to being mixed together for extrusion. The TCP shell and carbon core were finally put together to

manufacture a supply roll for extrusion at a temperature of 120 °C. The first filaments that passed through were cut, recharged, and extruded for the second filaments. The scaffolds obtained were carefully collected, burned, and finally sintered at 1100 °C for 2hr in an air atmosphere to avoid the formation of α-TCP during sintering. Then the pressure-less sintering was performed at 1350 °C for 2 h in an air atmosphere.

### 2.8. Preparation of experimental samples

The experimental samples were grouped as follows: hDBM, hDBM/DBM, hDBM/DBM/pTCP, and hDBM/DBM/gTCP. 15 w/v% of DBM was added to the hDBM, then 5 w/v% of pTCP and gTCP were loaded in the hDBM and DBM, respectively. The samples of each group were sterilized under UV for 1 h.

### 2.9. SEM analysis

Microstructure of hDBM, DBM, TCP powders, and TCP granules were observed by using a scanning electron microscope (SEM, JSM-6701F, Japan) in each sample group. SEM observation was carried out to investigate the microstructures of injectable bone grafts. The samples were freeze-dried and sputter coated with platinum (Cressington Scientific Instruments, UK) prior to examination.

### 2.10. Cell culture

The pre-osteoblast cells, MC3T3-E1 (ATCC, CRL-2593, US) were cultured in a growth medium with a minimum essential medium (α-mem, Welgene, Korea) which contained 10% fetal bovine serum (FBS, Corning, US) and 1% penicillin/streptomycin (PS, Welgene, Korea).

For the osteo-differentiation, MC3T3-E1 cells were cultured with an osteogenic medium, which consisted of α-mem, 10% FBS, 1% PS, 10 nM dexamethasone (Sigma, US), 10 μg/mL L-Ascorbic acid (Sigma, US), and 10 mM β-glycerophosphate disodium salt hydrate (Sigma, US). These cells were maintained at 37 °C in a 5% $CO_2$ incubator (Thermo Fisher Scientific, US).

### 2.11. Cell viability test

For evaluating the indirect cell viability, $10^4$ MC3T3-E1 cells were seeded onto each well of 24 well plates. All the samples were placed into a hanging insert well above the cells (SPLInsert™ Hanging 35124, SPL, Korea).

To verify cytotoxicity, after 1, 3, and 7 days of cell growth, the hanging insert well with samples was removed. 100 μl of 3-[4,5-dimethylthiazol-2-yl]-2,5-diphenyltetrazolium bromide (MTT, Sigma, USA) was added to the medium, which included cells. After 4 h of incubation, the medium was removed, 1 mL dimethyl sulfoxide (DMSO, Sigma, USA) was added, then it was incubated for 4 h. The optical density (OD) (200 μl of supernatant) was measured at 595 nm using an ELIZA plate reader (Bio-Tek, Korea). The cell proliferation (%) was calculated using Equation 2:

Cell proliferation (%) = (O.D values of sample/O. D values of control) x 100 (2)

For actin cytoskeleton staining, cells were fixed with 4% paraformaldehyde for 15 min, after 1, 3, and 7 days of incubation, blocked in 2.5% bovine serum albumin for 1 h, then stained with Alexa 488-conjugated phalloidin at 1 h and Hoechst for 5 min. The morphology of the cells spreading was observed under a confocal microscope (FV10i-W, Olympus, USA) using FV10-ASW 4.2 viewer software.

### 2.12. Western blot analysis

Cells seeded in wells containing samples in hanging insert wells were incubated for two days, then the medium was replaced with the osteogenic medium. They were then incubated for 7 and, 14 days and collected for Western blot analysis. Total protein was extracted using RIPA buffer (50 mM Tris-HCl, 150 mM NaCl, 1% NP40, 0.5% Sodium deoxycholate, 0.1% Sodium dodecyl sulfate, and 1% protease inhibitor); all these reagents were purchased from Sigma, US.

At first, cells were lysed in RIPA buffer for 30 min at 4 °C. To obtain the supernatant of lysed cells, centrifugation was done at 12,000 rpm for 20 min. The concentration of total protein of each sample was calculated using a protein assay dye reagent concentrate (Biorad, US) following the Bradford method. At that point, the same amount of protein was loaded onto 10% sodium dodecyl sulfate-polyacrylamide gel electrophoresis (SDS-PAGE, Biorad, US) and transferred into the polyvinylidene difluoride (PVDF, Biorad, US). Next, PVDF was blocked with 3% BSA for 1 h. Finally, PVDF was incubated with primary antibodies, Collagen 1 (COL1, Santacruz, US), Runt-related transcription factor 2 (RUNX2, Abcam, UK), and osteopontin (OPN, Novus, US) at 4 °C. Anti-β-actin (Santa Cruz, US) was used as a loading control for protein expressions across samples. After 24 h, membranes were again incubated with HRP-conjugated secondary antibodies of HRP-rabbit IgG (Cell Signaling, US) or HRP-mouse IgG (Cell Signaling, US) for 1 h at room temperature. The specific protein expressions were visualized using chemiluminescence (GE Health care, US) and ChemiDoc™ XRS+ (Biorad, US). We quantified the Western blot band image using Image J software (NIH, US).

### 2.13. In-vivo analysis

Male New Zealand White Rabbits (14 weeks old) were purchased from JSBIO (Korea). The animals were maintained under a temperature of 22 °C–24 °C and 12 h shift of the light-dark cycle. All procedures followed the rules of our Institutional Animal Care and Use Committee (Soonchunhyang University, South Korea). All surgical procedures were carried out under inhalational anesthesia using isoflurane (Piramal, India). The experiments were conducted in triplicate for each group. The rabbits were randomly grouped as follows: hDBM, hDBM/DBM, hDBM/DBM/pTCP, and hDBM/DBM/gTCP. After a septic preparation of the surgical field using 70% ethanol and povidone-iodine. an incision was made over the distal femoral head and a hole (5 mm × 6 mm) was then created in the femur using a trephine drill. Each scaffold was placed in the hole, by injecting using a syringe barrel (Inobone, Korea; shown in Fig 3 d-g), and the wound was then sutured. Antibiotics (Baytril, Bayer, Korea) and a painkiller (Maritrol, JEILPHARM, Korea) were administered for three days postoperatively. At 1 and, 2 months after implantation, animals were sacrificed, and the implanted site was harvested. All procedures were performed in accordance with the rules of our Institutional Animal Care and Use Committee (Approval number: SCH 22-0105)

### 2.14. Micro-CT analysis

At 1 month and 2 months after implantation, the rabbit femur was harvested for micro-CT analysis. The examinations were implemented by a Skyscan 1172 micro-CT scanner equipped with a software version 1.5, 11-megapixel camera (camera pixel size of 8.81 μm). The image acquisition was performed with a source voltage of 70 kV and current of 120 μA, image pixel size of 13.28 μm, and rotations of 360° with a step of 7°, with a flat-field correction. All data scans were processed via batch reconstruction using Nrecon software version 1.6.9.8. Standard data reconstruction was performed with corresponding ring artifact correction and post-alignment compensation. The resulting data sets were composed of bitmap image files measuring 2000 × 1336 pixels. Rotation and reorientation of the reconstructed data were performed using Data viewer software version 1.5.1. Percent bone volume [bone volume (BV)/tissue volume (TV) %] was determined as follows. Two regions of interest (ROIs) for each bone micro-CT image were selected. One is the entire defect area (TV), and the other is the bone matrix in the defect area (BV). For each thresholded ROI, we were able to calculate the BV/TV (%).

### 2.15. Histological examination

The extracted bone samples were fixed in a 10% neutral buffered formalin (Polyscience, Inc. US) for 3 days and decalcified with 5% nitric acid (Sigma, USA). The specimens were dehydrated serially with ethanol and embedded with paraffin. They were then sectioned at 5 μm using a microtome (Thermo-Scientific, USA) and placed on a coated slide glass. Next, the sections were stained with Harris's alum Hematoxylin and eosin and Masson's trichrome method to measure the collagen fibers [20]. Finally, they were visualized under an Olympus BX 53 microscope.

Immuno-histological staining was performed using primary antibodies and developed using a diaminobenzidine (DAB) substrate kit (Abcam, ab64238, UK), following the manufacturer's instructions. Briefly, sections were blocked with 3% BSA, then incubated with primary antibodies of CD68 (BioRad, USA) at 4 °C for 24 h. After washing them with wash buffer, samples were incubated with Envision/HRP antibody and DAB substrate chromogen solution in order to detect the specific protein as a deep brown color.

### 2.16. Statistical analysis

All experimental data are expressed as the mean ± standard deviation (SD). The Student's t-test was used to compare the data between two groups, and using two-way Analysis of Variance (ANOVA) with Tukey's multiple comparison test was conducted to compare the data from multiple groups. Statistical analyses were performed using the GraphPad Prism 5.0 program. The significance levels were $p < 0.001$***, $p < 0.01$**, $p < 0.05$*.

## 3. Results and discussion

### 3.1. Characterization of DBM

Fresh porcine bone particles were demineralized using acid extraction to remove the mineral content (Fig. 1a and b). The lipid was removed by chloroform/methanol, and an enzymatic decellularization procedure was applied with trypsin and EDTA to produce decellularized matrix particles (DBM) [19]. Effective decellularization of the tissue was confirmed with native bone matrix (NBM) (Fig. 1c) by reduction of the visible nuclei, as observed in hematoxylin and eosin (H&E) staining (Fig. 1d). Quantification of double-strand DNA (dsDNA) from NBM and DBM revealed the significant reduction in DBM of 3.43 ± 1.7 ng/mg (initial dry weight) whereas the content of dsDNA was quite high in NBM, 69.1 ± 3.4 ng/mg ($p < 0.005$) (initial dry weight; Fig. 1e). The residual DNA content of DBM was significantly lower than in the 50 ng of dsDNA which is a reference recommended for complete decellularization [21]. Correspondingly, there was no visible fragment of DNA in DBM while electrophoresed using 1% agarose gel (Fig. 1f), demonstrating successful decellularization.

Further, the presence of the essential growth factors such as BMP-2, TGF-β1, and VEGF in both NBM, as well as DBM, were measured, as shown in Fig. 1g. NBM showed 760.4 ± 14.7 pg/g of BMP-2, 712.1 ± 4.4 pg/g TGF-β1, and 605.2 ± 7.4 pg/g of VEGF, whereas DBM revealed 346.7 ± 20.1 pg/g of BMP-2, 152.2 ± 22.3 pg/g TGF-β1 and 57.5 ± 0.61 pg/g of VEGF. TGF-β1 is an important mitogenic factor, which modifies bone resorption as well as regeneration. VEGF stimulates both osteogenesis and angiogenesis, and BMP-2 is implicated in activating the endothelial cells for angiogenesis [22,23]. The concentration of the remaining growth factor in DBM was found much lower compared to NBM ($p < 0.001$), owing to successful demineralization and decellularization, on the other hand, there is a possibility that the exposed residual growth factor could be applied to host cells to promote osteogenesis [24].

### 3.2. Characterization of hDBM

DBM can be easily dissolved in organic solvents, so hydrogel of DBM can be made by pepsin. After neutralization with the physiological condition, hDBM can be formed thermo-sensitive hydrogel [19]. Although the hDBM can hold its shape in 37 °C conditions, it deforms easily under stress conditions.

After preparing the hDBM, the rheological characteristics of the hDBM were determined. The gelation of injectable hDBM happened after exposure to 37 °C as confirmed by the tube inversion test (Fig. 2a) and turbidimetric gelation (Fig. 2b). The $T_{lag}$, $T_{1/2}$, and $T_1$ were measured at 1.45 ± 0.34 min, 12.24 ± 0.78 min, and 18.03 ± 0.76 min, respectively. The gelation was started at 1.45 ± 0.34 min and the gelation of hDBM was fully formed after 18.03 ± 0.76 min at 37 °C. The viscosity was calculated using an increasing shear rate at 37 °C. The result showed that the viscosity decreased when the shear rate increased (from 1.25 Pa to 0.017Pa) (Fig. 2c). Additionally, the shear stress showed a decrease with increasing time (Fig. 2d). hDBM has the self-gelling ability at 37 °C after a certain time period under static conditions. Under stress this becomes fragile which is clearly evidenced by Fig. 2d. Due to the absence of crosslinking agent with hDBM, it became weak under rotation of the spindle while performing the experiment. In this study, hDBM was used to improve the sample injection capability. Moreover, thermo-sensitive DBM could prevent sample scattering during irrigation at surgical treatment.

Interestingly, growth factors were present even after digestion, the presence of the BMP-2, TGF-β1, and VEGF, in hDBM was measured, as shown in Fig. 2e. The concentrations of BMP-2, TGF-β1, and VEGF were 157.7 ± 1.76, 19.4 ± 5.7, and 15 ± 2.8 pg/ml, respectively.

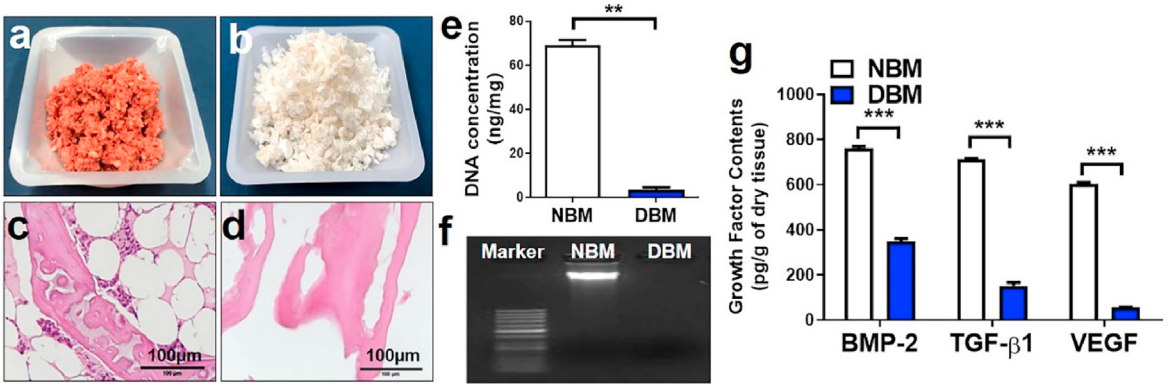


**Fig. 1.** Ground native bone matrix (NBM) (a) and demineralized bone matrix (DBM) after demineralization and decellularization (b). Hematoxylin and eosin staining of porcine bone before (c) and after demineralization and decellularization (d). DNA quantification in ng/mg of NBM and DBM (e), with gel electrophoresis to detect residual DNA before and after demineralization and decellularization (f). Growth factors (BMP-2, TGF-β1, and VEGF) quantification of NBM and DBM (g). (**, $p < 0.005$; ***, $p < 0.001$).

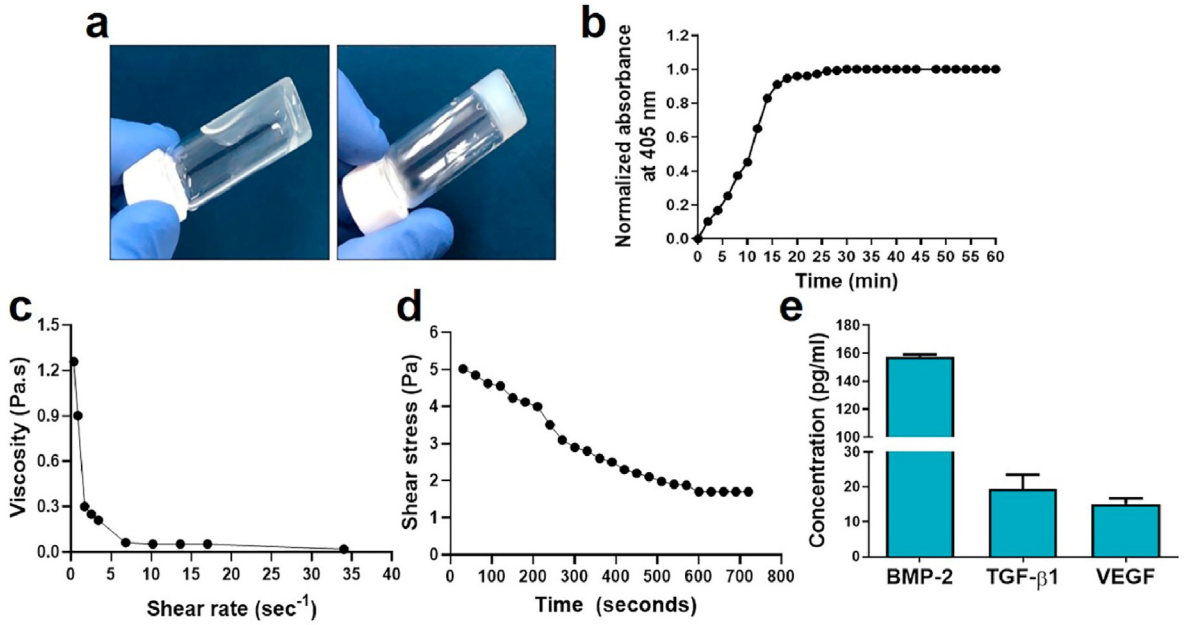


**Fig. 2.** Gelation and rheological properties of injectable DBM hydrogel (hDBM). Tube inversion test confirmed the gelation of thermosensitive hDBM after exposure at 37 °C (a). Representative curve of turbidimetric gelation of hDBM (b), change in viscosity at different shear rate (c), and change in shear stress of hDBM with respect to time (d). Growth factors (BMP-2, TGF-β1, and VEGF) quantification of hDBM (10 mg/ml) (e).

These results suggested that the use of thermo-sensitive gelation-forming hDBM improves injection performance, allowing samples to be easily applied to defects. And residual growth factors in hDBM could promote bone healing.

### 3.3. Microstructure of graft samples

In the present study, a combination of DBM and TCP has been prepared, which would probably create a composite with improved osteoconductivity and osteoinductivity. TCP powder and TCP granules (each 15 w/v %) were applied in hDBM and DBM. Fig. 3a–c shows the microstructure of DBM, pTCP and gTCP. Fig. 3d–g represents the photographs of hDBM, hDBM/DBM, hDBM/DBM/pTCP, and hDBM/DBM/gTCP grafts prepared with an injectable type that provides easy-to-handle implants. Those graft types were made possible by the loading of thermosensitive hDBM.

Microstructure of lyophilized samples of hDBM, hDBM/DBM, hDBM/DBM/pTCP, and hDBM/DBM/gTCP were investigated to confirm the morphology and distribution of hDBM, DBM, and TCPs (Fig. 3h–k). The hDBM showed typical hydrogel morphologies of fibrous ECM structures in all bone-graft samples as indicated in yellow arrows. Also, DBM, pTCP, and gTCP of distribution (red arrows, blue stars, and green dotted line, respectively) were found among hDBM nanofibers that appeared to interconnect pores. The high magnification images of hDBM and DBM revealed distinctively smooth surfaces (Fig. 3h-I, SI:Fig SI.2a). It was found that the micron-sized pTCP was well distributed within composite DBM and hDBM (Fig. 3j, SI:Fig SI.2b) and gTCP exhibited a granular structure including micropores without any irregularities (Fig. 3k).

### 3.4. Cell viability and cell proliferation

To assess the cytocompatibility of hDBM, hDBM/DBM, hDBM/DBM/pTCP, and hDBM/DBM/gTCP grafts, the samples were seeded with pre-osteoblast cells (MC3T3-E1). For cellular viability and proliferation, the MTT assay was evaluated after 1, 3, and 7 days of incubation (Fig. 4a). The cell viability showed no significant differences between the hDBM, hDBM/DBM, hDBM/DBM/pTCP, and hDBM/DBM/gTCP samples.

The cellular proliferation was also evaluated by using confocal microscope imaging showing the f-actin (green) and Hoechst (blue) expressions of the seeded cells after 1, 3, and 7 days of incubation (Fig. 4b).

The results showed that the number of seeded cells increased over time, and cells were connected to each other on all scaffolds during the culture periods. The hDBM and DBM provided an ECM environment, which could support cell proliferation and differentiation [25]. ECM is important for cell growth and vascularization eases the passage of nutrients [26,27]. Also, earlier studies showed that TCP leads to excellent cellular attachment and migration [28]. These results indicated that the loading of TCP and soluble ECM components retained in DBM and DBM hydrogel-based samples facilitated suitable cellular niches for cell-cell interaction and migration.

### 3.5. Western blot analysis

To examine the effect of hDBM, hDBM/DBM, hDBM/DBM/pTCP, and hDBM/DBM/gTCP bone grafts on osteogenic differentiation, each sample was cultured with MC3T3-E1 cells under osteogenic-differentiation medium conditions for 7 and 14 days (Fig. 5a). COL1 and Runx2 expressions were evaluated for an early-stage of osteogenic differentiation marker [29,30]. As shown in Fig. 5b, only COL1 was equally expressed in all experimental groups at 7 days and 14 days. hDBM/DBM/pTCP and hDBM/DBM/gTCP, which consist of TCP, RUNX2 was highly expressed at 7 days and 14 days ($p < 0.001$) (Fig. 5c). The explanation of these phenomena lay in the increasing ability of the hDBM/DBM/pTCP and hDBM/DBM/gTCP samples to release calcium and phosphorus ions into the medium. The existence of the calcium phosphate helped in better mineralization by means of RUNX2 expression and hence induced differentiation of pre-osteoblast cells [31,32]. Moreover, since the release of calcium and phosphorus ions was higher in pTCP (SI:Fig SI.1) than in gTCP, hDBM/DBM/pTCP showed higher expression of RUNX2 compared with hDBM/DBM/gTCP. The presence/release of calcium phosphates plays essential roles in cell adhesion and tissue formation by affecting the adsorption of extracellular matrix proteins on the surface [16]. Their properties also influence bone regeneration by affecting newly formed bone minerals [32].

The expression of OPN is mainly associated with bone metabolism and remodeling and relatively late-stage osteogenic differentiation [33].

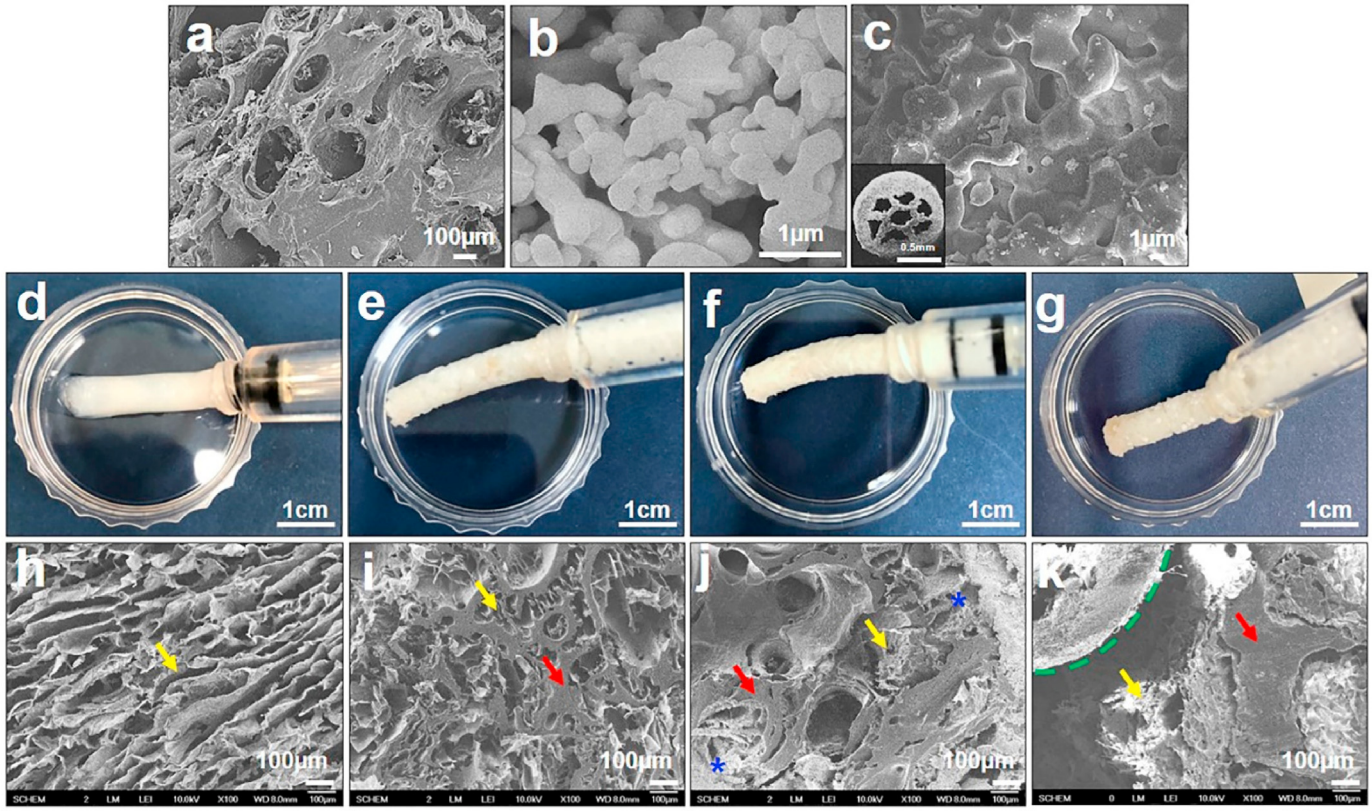


**Fig. 3.** Scanning electron microscopy (SEM) images for DBM (a), pTCP (b), and gTCP (c). Injectable hDBM (d), hDBM/DBM (e), hDBM/DBM/pTCP (f), and hDBM/DBM/gTCP (g) bone grafts and its SEM images of hDBM (h), hDBM/DBM (i), hDBM/DBM/pTCP (j) and hDBM/DBM/gTCP (k). (yellow arrows, hDBM; red arrows, DBM; blue stars, pTCP; green dotted line, gTCP). (For interpretation of the references to color in this figure legend, the reader is referred to the Web version of this article.)

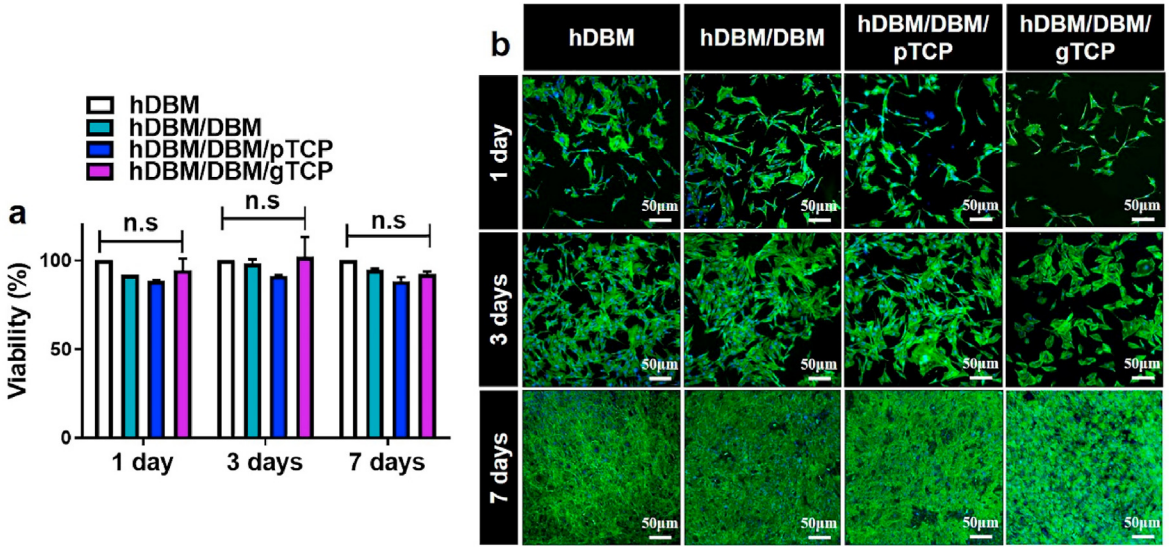


**Fig. 4.** Cell viability of bone grafts were determined by MTT assay (a) and cell proliferation behavior (b) after an incubation of 1, 3, and 7 days. F-actin and nucleus are expressed by green and blue colors, respectively. (n.s: not significant). (For interpretation of the references to color in this figure legend, the reader is referred to the Web version of this article.)

Its expression showed higher values in the hDBM, hDBM/DBM, hDBM/DBM/pTCP, and hDBM/DBM/gTCP groups than in the control at 14 days ($p < 0.001$) (Fig. 5D). The reasons can be inferred from the exposure of growth factors in all experimental samples. B. Zhao et al. reported that OPN is stimulated by growth factors such as BMP2 to promote differentiation for osteoblasts [34]. As indicated above, residual BMP-2 levels in DBM and hDBM were measured. Exposed BMP-2 might promote osteogenic biomolecules and improve osteogenic

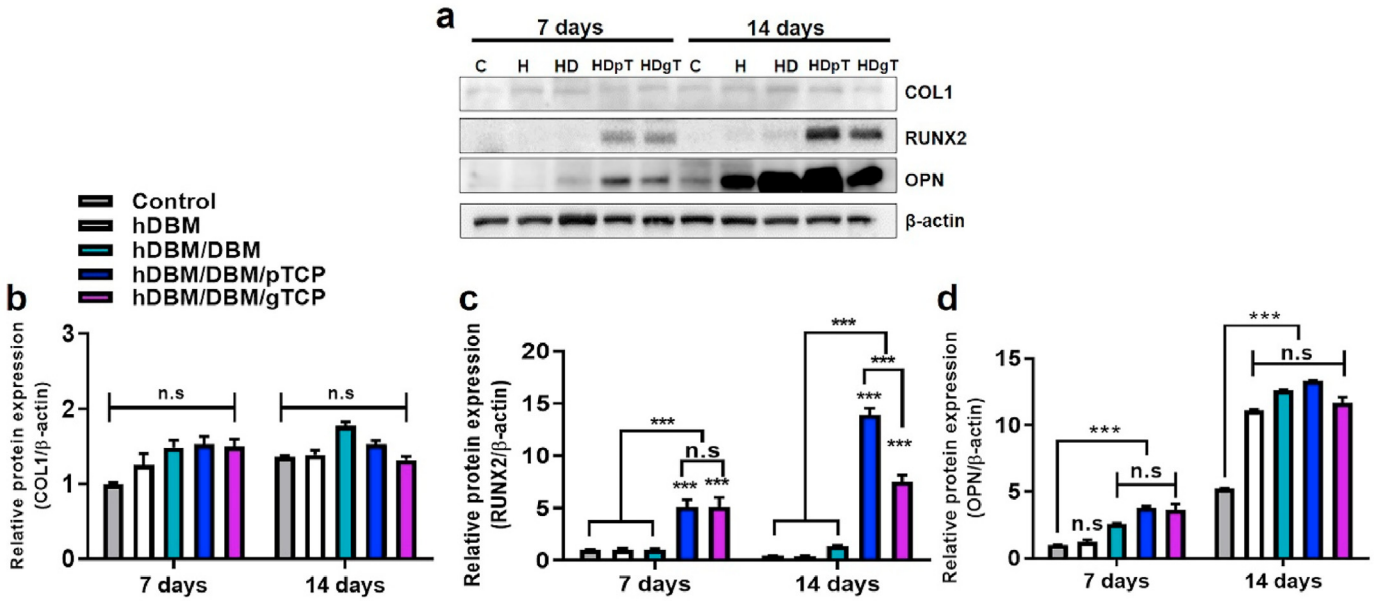


**Fig. 5.** Osteogenic differentiation-related protein expressions in MC3T3E-1 cells. Evaluation of COL1, RUNX2, and OPN expressions by western blot analysis (a) and their quantification analysis of COL1 (b), RUNX2 (c), and OPN (d). (C, without samples; H, hDBM; HD, hDBM/DBM; HDpT, hDBM/DBM/pTCP; HDgT, hDBM/DBM/gTCP) (n.s, not significant; ***, $p < 0.001$).

differentiation. These findings indicate that TCP-loaded hDBM/DBM bone grafts could contribute to bone regeneration.

### 3.6. Micro-CT analysis

To analyze the *in-vivo* bone formation, we implanted hDBM, hDBM/DBM, hDBM/DBM/pTCP, and hDBM/DBM/gTCP grafts using the rabbit-femur defect model for 1 month and 2 months. Bone defects 6 mm in diameter and 5 mm in length were created in the femoral bones of the rabbit and then implanted with the different scaffolds, as shown in Fig. 6a and b.

The new bone formation of the different bone grafts was evaluated by 3D micro-CT image analysis. New bone formation was measured by quantitative analysis of percentages of bone volume in total tissue volume (BV/TV, %). As shown in Fig. 6c, no significant differences were observed in any experimental group 1 month after implantation. At 2 months after implantation, the percentages of BV/TV were 23 ± 8.1%, 36.1 ± 0.7%, 24.6 ± 3.9%, and 45.2 ± 6.3% in hDBM, hDBM/DBM, hDBM/DBM/pTCP and hDBM/DBM/gTCP, respectively. Interestingly, the highest BV/TV percentage was in the hDBM/DBM/gTCP implanted samples, whereas hDBM/DBM/pTCP showed the lowest values ($p < 0.05$) except hDBM.

The reconstructed micro-CT images (Fig. 6d) indicated that hDBM/DBM/gTCP implantation after 2 months showed an increase in bone formation at the defect site compared to 1 month. On the other hand, hDBM/DBM/pTCP showed a pattern in which the defect site increased with the empty area found wider at 2 months than at 1 month. This finding confirms that the hDBM/DBM/gTCP bone transplant has the potential for bone regeneration.

Surprisingly, our findings were different from our hypothesis by

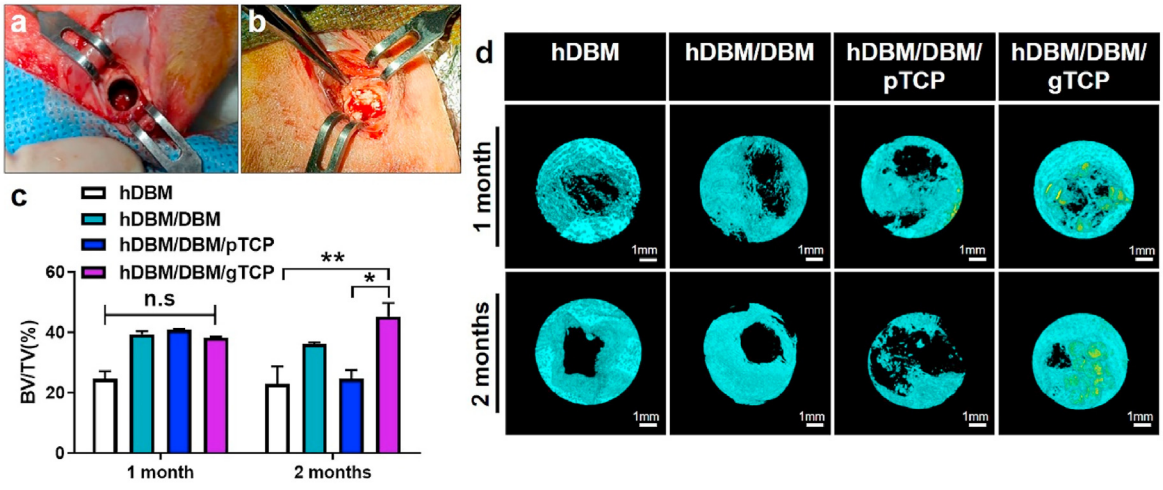


**Fig. 6.** Images showing femur defect site in rabbit (a), and implantation of bone grafts in defect (b). Quantitative analysis of regenerated bone volume fraction in total tissue volume (BV/TV, %) for each sample (c). 3D reconstructed micro-CT images of implanted femur bone region after bone grafts implantation for 1 month and 2 months (d). Light blue indicates newly formed bone and yellow indicates materials. (n.s, not significant; *, $p < 0.05$; **, $p < 0.005$; scale bar = 1 mm). (For interpretation of the references to color in this figure legend, the reader is referred to the Web version of this article.)

means of DBM and TCP combination. The hDBM/DBM/pTCP and hDBM/DBM/gTCP may have influenced the defect sites by different mechanisms. Micro-CT analysis has limitations in distinguishing between implanted grafts and newly formed bone; therefore, it was further evaluated by histological analysis.

### 3.7. Histological analysis

To evaluate the new bone formation, we used H&E staining of the different implanted grafts (Figs. 7 and 8). In the hDBM implantation, new bone formation was initiated but mostly filled with bone-marrow-like structures even after 2 months. Although hDBM had residual growth factors, this was insufficient for bone growth. (Fig. 7a, e).

The hDBM/DBM implanted site was filled with un-resorbed DBM after 1 month of implantation (Fig 7b). After 2 months of implantation, small amounts of newly formed bone appeared with the thin trabecular bone structure (Fig. 7f). Due to the early resorption of DBM, its scaffolding role cannot be expected until sufficient bone formation occurs. This phenomenon is usually found as a subsidence of dental implants in the clinical field when DBM has been implanted alone [35].

In hDBM/DBM/pTCP and hDBM/DBM/gTCP, which were loaded with synthetic TCP, implanted DBM was found with empty lacunae, as indicated by black arrows at both grafts (Fig. 8a–d). Interestingly, hDBM/DBM/pTCP implanted site was filled with dense fibrous tissue, which was similar in structure to fibrous dysplasia after 2 months of implantation (Fig. 8e and f). On the other hand, the hDBM/DBM/gTCP implanted site

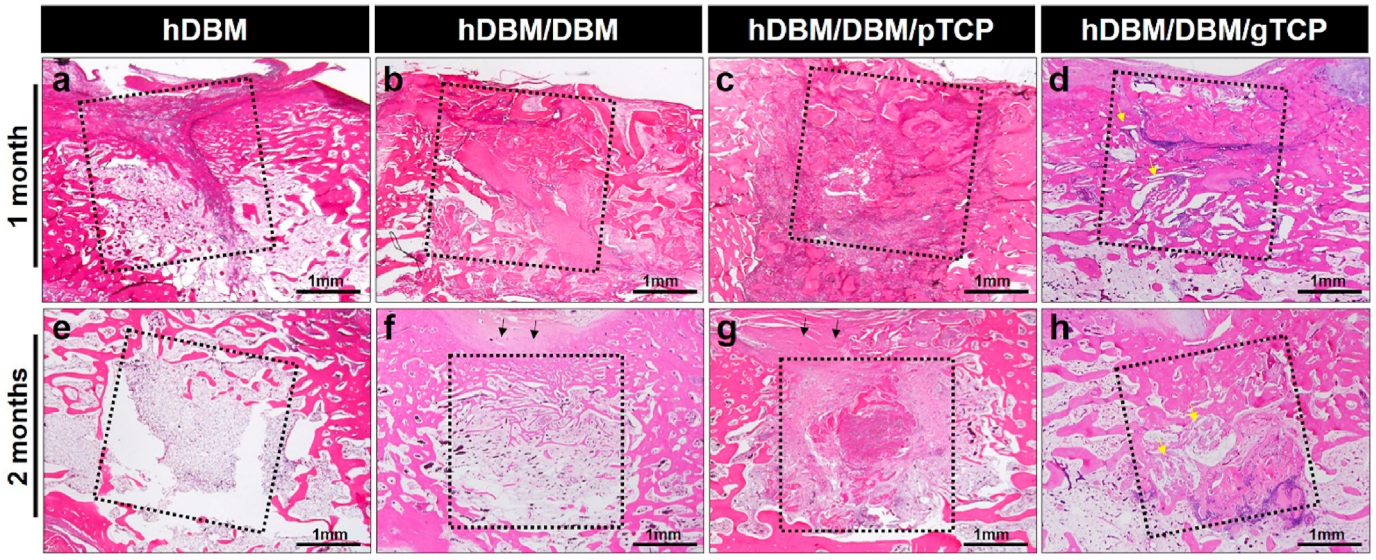


**Fig. 7.** Histological analysis of the hDBM (a, e), hDBM/DBM (b, f), hDBM/DBM/pTCP (c, g), and hDBM/DBM/gTCP (d, h) bone grafts in the femur defect model at 1 month and 2 months after implantation. (dot box, graft implanted site; black arrows, collapsed tissue; yellow arrows, gTCP; scale bar = 1 mm). (For interpretation of the references to color in this figure legend, the reader is referred to the Web version of this article.)

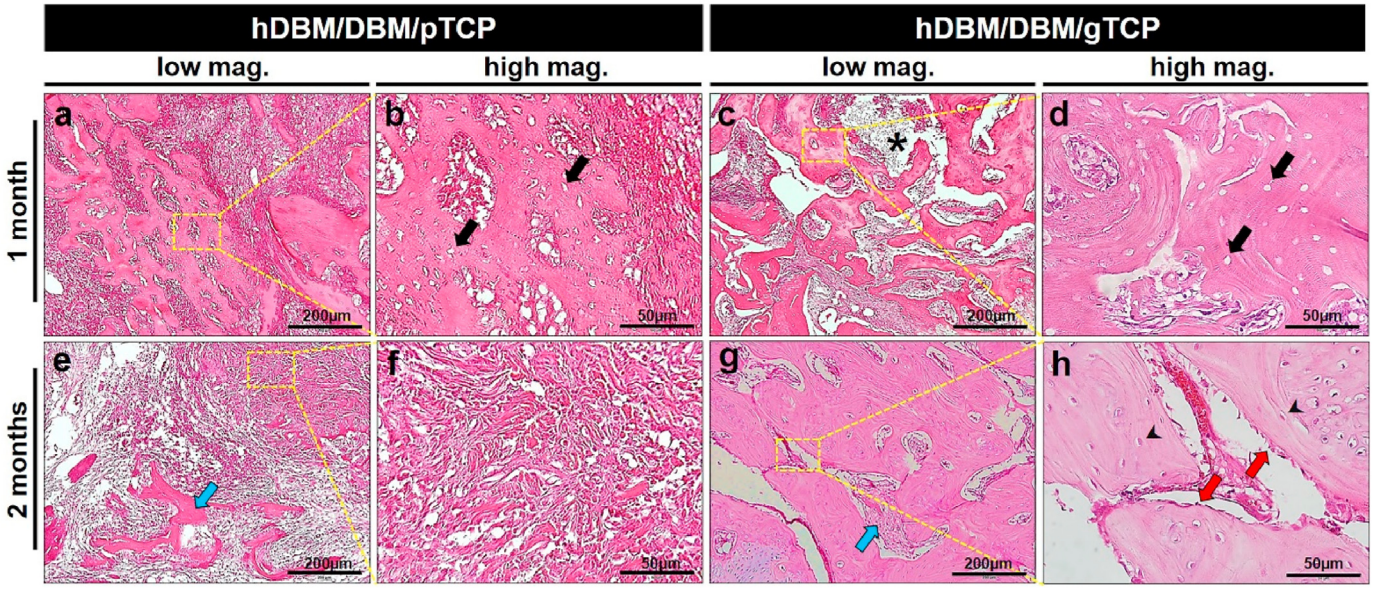


**Fig. 8.** Hematoxylin & eosin (H&E) stained images of the hDBM/DBM/pTCP and hDBM/DBM/gTCP bone grafts in the femur defect model at 1 month and 2 months after implantation. Images showed the DBM with empty lacunae in hDBM/DBM/pTCP (a, b) and hDBM/DBM/gTCP (c, d) grafts implanted areas at 1 month. After 2 months implantation of hDBM/DBM/pTCP (e, f) and hDBM/DBM/gTCP (g, h) grafts showed fibrous dysplasia-like structures and bone formation, respectively. (scale bar: low magnification = 200 μm; high magnification = 50 μm) (arrows, empty lacunae; arrow heads, osteocyte; star, degraded gTCP; blue arrows, resorbed DBM; red arrows, osteoblast). (For interpretation of the references to color in this figure legend, the reader is referred to the Web version of this article.)

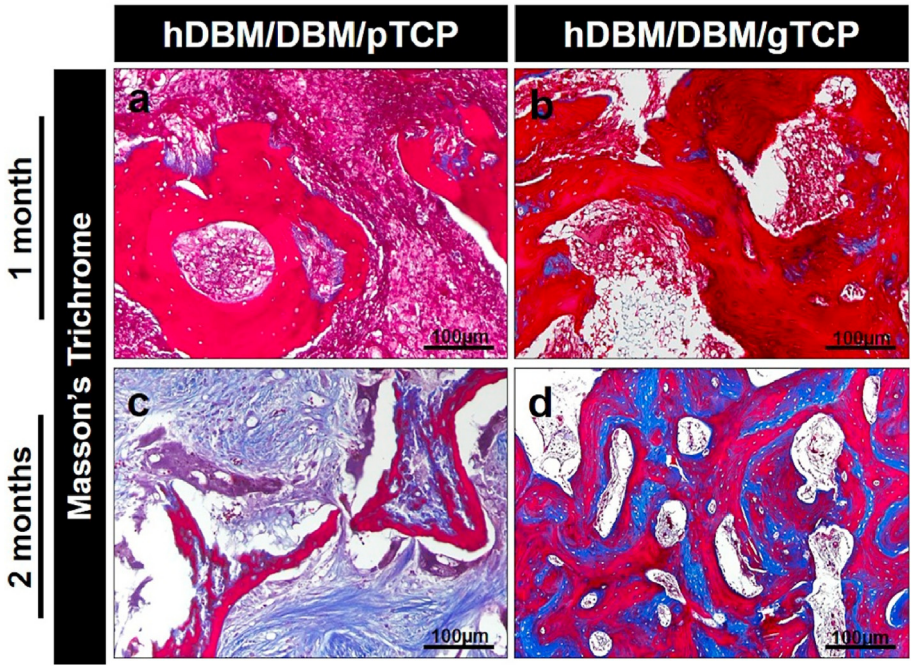


**Fig. 9.** Masson's trichrome stained images showed the areas of demineralized bone matrix (red-stained areas) and collagen distributions (blue-stained areas) in the hDBM/DBM/pTCP (a, c) and hDBM/DBM/gTCP (b, d) implanted areas at 1 month and 2 months after implantation. (scale bar = 100 μm). (For interpretation of the references to color in this figure legend, the reader is referred to the Web version of this article.)

revealed new bone formed with osteoblasts and osteocytes with the degraded gTCP (Fig. 8g and h).

Masson-Trichrome staining was also carried out after 1 month and 2 months of implantation for hDBM/DBM/pTCP and hDBM/DBM/gTCP grafts, as indicated in Fig. 9a–d. The DBM is shown in each implanted site in red colored areas, and newly grown bone is represented in blue color after 2 months of implantation. Newly formed bone is shown in the hDBM/DBM/gTCP implanted site in blue within the bone marrow, whereas the hDBM/DBM/pTCP showed resorbed DBM and collagen fibers, as can be found in fibrous dysplasia-like structures.

As mentioned above, there are limitations to the use of DBM alone as a bone graft, because of the early resorption caused by the lack of calcium and phosphate. Therefore, a material that can serve as a scaffolding for the defect area is also required. As expected, the mixture of DBM and TCP exhibited excellent bone formation by a synergistic effect, which in our case corresponds to the hDBM/DBM/gTCP graft. In our previous study, gTCP showed excellent bone formation after 6 months in a rabbit-femur defect model [18]. Multichannel porous gTCP provided sufficient

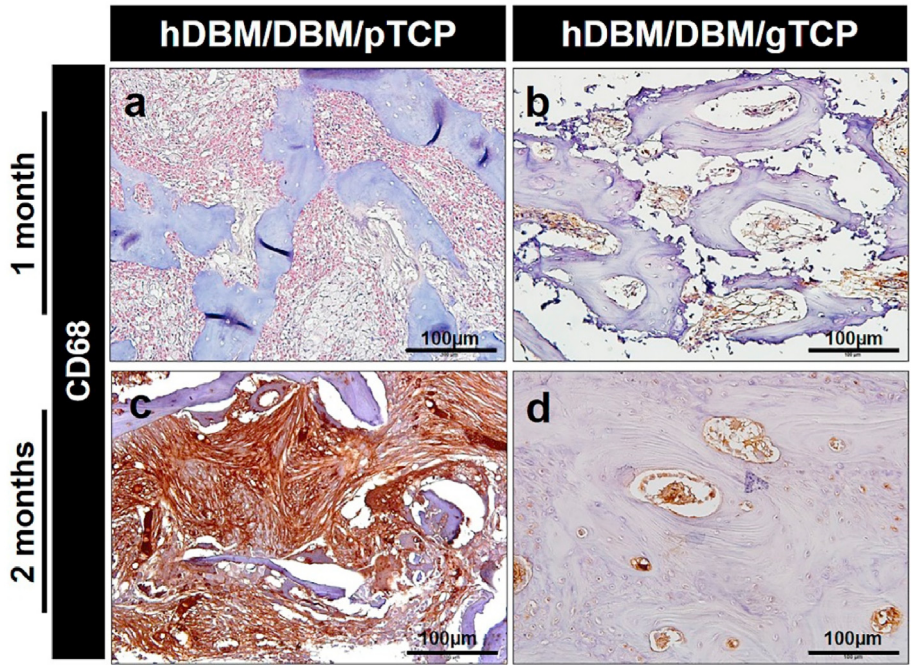


**Fig. 10.** Representative immunohistochemical 3′-Diaminobenzidine (DAB) staining images of CD68 in the hDBM/DBM/pTCP and hDBM/DBM/gTCP implanted areas at 1 month (a–b) and 2 months (c–d) after implantation. (Scale bar = 100 μm).

scaffolding to allow bone formation. Interestingly, compared to 6 months after implantation of gTCP, hDBM/DBM/gTCP graft showed better bone formation within 2 months after implantation. The result indicated that gTCP has a synergistic effect while mixed with DBM and hDBM, which have osteoinductive properties due to the presence of growth factors.

However, the pTCP results were not as expected. According to our results, fibrous dysplasia-like structures were observed at the hDBM/DBM/pTCP implanted site, which showed collagen fibers and fibrous tissues. Fibrous dysplasia is an uncommon bone disease in which normal bone marrow is replaced by fibrous bone tissue, causing bone deformity, fracture, and pain [36]. There are few reports to support our findings. Harris WH et al. reported that wear particles cause aseptic loosening in the total hip-joint replacement and induce bone resorption and osteolysis by means of induced phagocytosis of macrophages [37]. Moreover, Tobias Lange et al. showed that micron-sized TCP particles could induce the production of pro-inflammatory cytokines, and TCP particles could lead to particle-induced inflammation [38].

To investigate inflammatory reactions, DAB staining has been performed to evaluate macrophage expression on the hDBM/DBM/pTCP and hDBM/DBM/gTCP implanted sites after 1 month and 2 months of implantation. As shown in Fig. 10, the expression of CD68 was indicated by its brown color. CD68 is a protein that can be highly expressed by cells in the monocyte lineage, for example, macrophages, which are a proinflammation marker [39]. The hDBM/DBM/pTCP showed higher expressions of CD68 than that of the hDBM/DBM/gTCP at 1 month and 2 months. In particular, CD68 was strongly expressed throughout the fibrous tissue in hDBM/DBM/pTCP. The results showed that macrophages were induced in response to TCP powder in hDBM/DBM/pTCP grafts.

The histopathological differences between hDBM/DBM/pTCP and hDBM/DBM/gTCP can be explained via schematic illustration in Fig. 12. As expected from the above results, different cellular mechanisms were followed by the pTCP and gTCP. In the initial stage of implantation, a foreign body reaction begins in defect sites [40]. Subsequently, macrophages and osteoclasts were induced as an inflammatory response [41,42]. In hDBM/DBM/pTCP, osteoclasts played the role in the resorption of

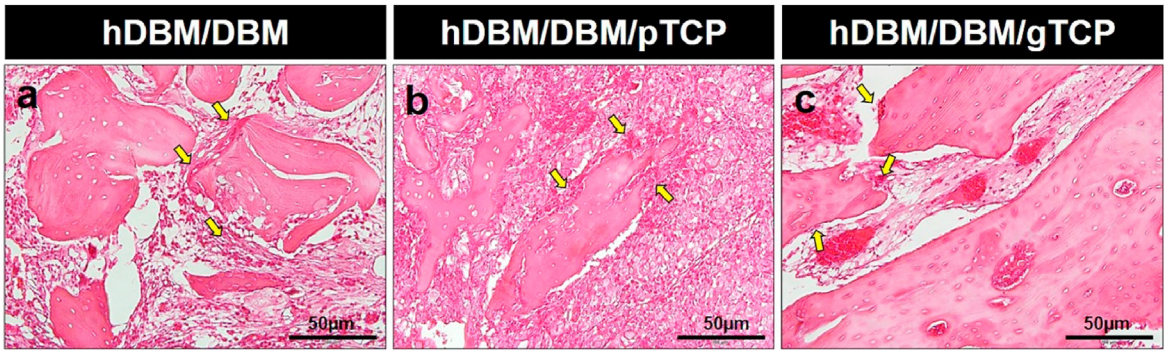


**Fig. 11.** Hematoxylin & eosin (H&E) staining images of osteoclast found in bone graft samples containing DBM at 1month after implantations of hDBM/DBM (a), hDBM/DBM/pTCP (b) and hDBM/DBM/gTCP (c). Yellow arrows indicate osteoclast. (Scale bar = 50 μm). (For interpretation of the references to color in this figure legend, the reader is referred to the Web version of this article.)

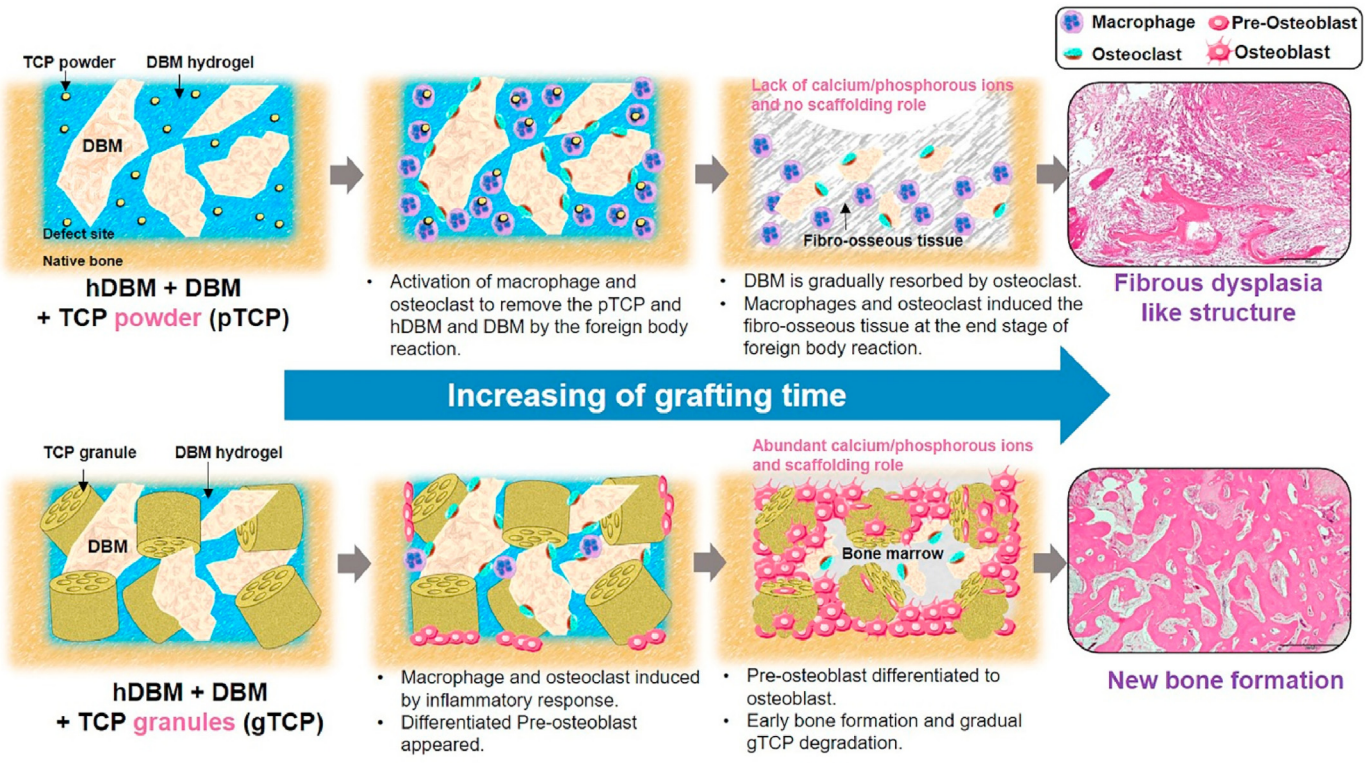


**Fig. 12.** Cellular mechanisms according to powder and granular morphology of tricalcium phosphate in injectable demineralized bone matrix particles and hydrogels.

DBM (Fig. 11) and macrophages were activated to eliminate TCP powder. Because of the high expression of macrophages, the normal healing process did not take place. Eventually, the induced macrophages stimulate fibrosis by secreting cytokines leading to the formation of fibrous tissue [43]. In addition, the TCP powder was removed by macrophages and formation of fibrous dysplasia-like structure took place instead of bone formation.

In the case of hDBM/DBM/gTCP, osteoclasts and macrophages were also induced by the inflammatory response, but those cells affect only the resorption of DBM. In addition, the DBM performs the intrinsic osteoinduction mechanism by releasing growth factors such as BMP2 by means of DBM resorption [44]. Even with the DBM resorbed, gTCP acted as a scaffold at the defect site until the new bone perfectly occurred. In addition, appropriate degradation of gTCP provided an environment where calcium and phosphate were released on a sustainable basis. Porous multi-channel gTCP can also accelerate the process of bone regeneration by promoting the biological activity of osteoblasts and rapid angiogenesis [18]. Eventually, with the normal healing process, new bones were formed along with the presence of osteoblasts differentiated from pre-osteoblasts.

## 4. Conclusion

The injectable type of bone graft was prepared using thermosensitive DBM hydrogel loaded with DBM and TCP to increase its osteoinductivity and osteoconductivity. Principally, a comparative study was conducted by mixing different morphologies of TCP (gTCP and pTCP) with hDBM and DBM respectively. The hDBM/DBM/pTCP and hDBM/DBM/gTCP showed biocompatibility and highly expressed differentiation markers such as Runx2 and OPN using a pre-osteoblast cell line. *In-vivo* studies showed that hDBM/DBM/gTCP revealed excellent bone formation, whereas hDBM/DBM/pTCP appeared to be filled with fibrous tissues and collagen fibers like fibrous dysplasia structure after 2 months of implantation. Macrophage activation was confirmed by the high expression of the CD 68 marker for hDBM/DBM/pTCP. The results confirmed that hDBM/DBM/gTCP might induce new bone formation as a scaffolding role of gTCP. In addition, gTCP exhibited a synergistic effect on bone formation by loading growth factors containing DBM/hDBM. However, hDBM/DBM/pTCP caused inflammation by pTCP-induced macrophages, resulting in a fibrous dysplasia-like structure. This finding could be used as guidelines for the study of DBM and TCP mixture grafts.

## Credit author statement

Hoe-Jin Kang: Investigation, Validation, Methodology, visualization, Writing - original draft. Seong-Su Park: Investigation, Validation, visualization. Garima Tripathi: Validation, Writing - review & editing. Byong-Taek Lee: Supervision, Conceptualization, Writing - review & editing, Funding acquisition, Project administration.

## Declaration of competing interest

The authors declare that they have no known competing financial interests or personal relationships that could have appeared to influence the work reported in this paper.

## Data availability

The authors do not have permission to share data.

## Acknowledgment

We disclose receipt of the following financial support for the research, authorship, and/or publication of this article. This research study was supported by a grant (2015R1A6A1A03032522) of the Basic Science Research Program through the National Research Foundation (NRF) funded by the Ministry of Education. It was also partially supported by Soonchunhyang University, South Korea.

## Appendix A. Supplementary data

Supplementary data to this article can be found online at https://doi.org/10.1016/j.mtbio.2022.100422.

## References

[1] M.T. Spang, K.L. Christman, Extracellular matrix hydrogel therapies: in vivo applications and development, Acta Biomater. 68 (2018) 1–14.
[2] L.T. Saldin, M.C. Cramer, S.S. Velankar, L.J. White, S.F. Badylak, Extracellular matrix hydrogels from decellularized tissues: structure and function, Acta Biomater. 49 (2017) 1–15.
[3] A. Gilpin, Y. Yang, Decellularization strategies for regenerative medicine: from processing techniques to applications, BioMed Res. Int. 2017 (2017).
[4] H. Zhang, L. Yang, X.g. Yang, F. Wang, J.t. Feng, K.c. Hua, Q. Li, Y.c. Hu, Demineralized bone matrix carriers and their clinical applications: an overview, Orthop. Surg. 11 (5) (2019) 725–737.
[5] H. Geckil, F. Xu, X. Zhang, S. Moon, U. Demirci, Engineering hydrogels as extracellular matrix mimics, Nanomedicine 5 (3) (2010) 469–484.
[6] X. Ding, X. Wei, Y. Huang, C. Guan, T. Zou, S. Wang, H. Liu, Y. Fan, Delivery of demineralized bone matrix powder using a salt-leached silk fibroin carrier for bone regeneration, J. Mater. Chem. B 3 (16) (2015) 3177–3188.
[7] F.-M. Chen, X. Liu, Advancing biomaterials of human origin for tissue engineering, Prog. Polym. Sci. 53 (2016) 86–168.
[8] M. Dang, L. Saunders, X. Niu, Y. Fan, P.X. Ma, Biomimetic delivery of signals for bone tissue engineering, Bone Res. 6 (1) (2018) 1–12.
[9] H. Capella-Monsonís, M. Tilbury, J. Wall, D. Zeugolis, Porcine mesothelium matrix as a biomaterial for wound healing applications, Mater. Today Bio. 7 (2020), 100057.
[10] M.W. Tibbitt, K.S. Anseth, Hydrogels as extracellular matrix mimics for 3D cell culture, Biotechnol. Bioeng. 103 (4) (2009) 655–663.
[11] S. Datta, A.P. Rameshbabu, K. Bankoti, M. Roy, C. Gupta, S. Jana, A.K. Das, R. Sen, S. Dhara, Decellularized bone matrix/oleoyl chitosan derived supramolecular injectable hydrogel promotes efficient bone integration, Mater. Sci. Eng. C 119 (2021), 111604.
[12] V.A.S. David, V.R. Güiza-Argüello, M.L. Arango-Rodríguez, C.L. Sossa, S.M. Becerra-Bayona, Decellularized tissues for wound healing: towards closing the gap between scaffold design and effective extracellular matrix remodeling, Front. Bioeng. Biotechnol. 10 (2022).
[13] D. Gothard, E.L. Smith, J.M. Kanczler, C.R. Black, J.A. Wells, C.A. Roberts, L.J. White, O. Qutachi, H. Peto, H. Rashidi, In vivo assessment of bone regeneration in alginate/bone ECM hydrogels with incorporated skeletal stem cells and single growth factors, PLoS One 10 (12) (2015), e0145080.
[14] G. Fernandez de Grado, L. Keller, Y. Idoux-Gillet, Q. Wagner, A.-M. Musset, N. Benkirane-Jessel, F. Bornert, D. Offner, Bone substitutes: a review of their characteristics, clinical use, and perspectives for large bone defects management, J. Tissue Eng. 9 (2018), 2041731418776819.
[15] R. Zhao, R. Yang, P.R. Cooper, Z. Khurshid, A. Shavandi, J. Ratnayake, Bone grafts and substitutes in dentistry: a review of current trends and developments, Molecules 26 (10) (2021) 3007.
[16] J. Jeong, J.H. Kim, J.H. Shim, N.S. Hwang, C.Y. Heo, Bioactive calcium phosphate materials and applications in bone regeneration, Biomater. Res. 23 (1) (2019) 1–11.
[17] M.-P. Ginebra, M. Espanol, Y. Maazouz, V. Bergez, D. Pastorino, Bioceramics and bone healing, EFORT Open Rev. 3 (5) (2018) 173–183.
[18] H.-J. Kang, P. Makkar, A.R. Padalhin, G.-H. Lee, S.-B. Im, B.-T. Lee, Comparative study on biodegradation and biocompatibility of multichannel calcium phosphate based bone substitutes, Mater. Sci. Eng. C 110 (2020), 110694.
[19] M.J. Sawkins, W. Bowen, P. Dhadda, H. Markides, L.E. Sidney, A.J. Taylor, F.R. Rose, S.F. Badylak, K.M. Shakesheff, L.J. White, Hydrogels derived from demineralized and decellularized bone extracellular matrix, Acta Biomater. 9 (8) (2013) 7865–7873.
[20] A. Ozawa, M. Sakaue, New decolorization method produces more information from tissue sections stained with hematoxylin and eosin stain and masson-trichrome stain, Ann. Anat. Anatomischer Anzeiger 227 (2020), 151431.
[21] P.M. Crapo, T.W. Gilbert, S.F. Badylak, An overview of tissue and whole organ decellularization processes, Biomaterials 32 (12) (2011) 3233–3243.
[22] K. Hu, B.R. Olsen, The roles of vascular endothelial growth factor in bone repair and regeneration, Bone 91 (2016) 30–38.
[23] X. Xu, L. Zheng, Q. Yuan, G. Zhen, J.L. Crane, X. Zhou, X. Cao, Transforming growth factor-β in stem cells and tissue homeostasis, Bone research 6 (1) (2018) 1–31.
[24] M.S. Lee, D.H. Lee, J. Jeon, G. Tae, Y.M. Shin, H.S. Yang, Biofabrication and application of decellularized bone extracellular matrix for effective bone regeneration, J. Ind. Eng. Chem. 83 (2020) 323–332.
[25] H. Amirazad, M. Dadashpour, N. Zarghami, Application of decellularized bone matrix as a bioscaffold in bone tissue engineering, J. Biol. Eng. 16 (1) (2022) 1–18.
[26] V. Poltavets, M. Kochetkova, S.M. Pitson, M.S. Samuel, The role of the extracellular matrix and its molecular and cellular regulators in cancer cell plasticity, Front. Oncol. 8 (2018) 431.
[27] D. Hao, H.S. Swindell, L. Ramasubramanian, R. Liu, K.S. Lam, D.L. Farmer, A. Wang, Extracellular matrix mimicking nanofibrous scaffolds modified with mesenchymal

stem cell-derived extracellular vesicles for improved vascularization, Front. Bioeng. Biotechnol. 8 (2020) 633.
[28] E. Cichoń, K. Haraźna, S. Skibiński, T. Witko, A. Zima, A. Ślósarczyk, M. Zimowska, M. Witko, B. Leszczyński, A. Wróbel, Novel bioresorbable tricalcium phosphate/polyhydroxyoctanoate (TCP/PHO) composites as scaffolds for bone tissue engineering applications, J. Mech. Behav. Biomed. Mater. 98 (2019) 235–245.
[29] J. Xu, Z. Li, Y. Hou, W. Fang, Potential mechanisms underlying the Runx2 induced osteogenesis of bone marrow mesenchymal stem cells, Am. J. Tourism Res. 7 (12) (2015) 2527.
[30] S. Kannan, J. Ghosh, S.K. Dhara, Osteogenic differentiation potential of porcine bone marrow mesenchymal stem cell subpopulations selected in different basal media, Biol. open 9 (10) (2020) bio053280.
[31] W. Chen, H. Zhou, M.D. Weir, M. Tang, C. Bao, H.H. Xu, Human embryonic stem cell-derived mesenchymal stem cell seeding on calcium phosphate cement-chitosan-RGD scaffold for bone repair, Tissue Eng. 19 (7–8) (2013) 915–927.
[32] Y. Nakagawa, T. Muneta, K. Tsuji, S. Ichinose, Y. Hakamatsuka, H. Koga, I. Sekiya, β-Tricalcium phosphate micron particles enhance calcification of human mesenchymal stem cells in vitro, J. Nanomater. 2013 (2013).
[33] J. Si, C. Wang, D. Zhang, B. Wang, W. Hou, Y. Zhou, Osteopontin in bone metabolism and bone diseases, e919159, Med. Sci. Mon. Int. Med. J. Exp. Clin. Res.: Int. Med. J. Exp. Clin. Res. 26 (2020) 1.
[34] B. Zhao, G. Xing, A. Wang, The BMP signaling pathway enhances the osteoblastic differentiation of bone marrow mesenchymal stem cells in rats with osteoporosis, J. Orthop. Surg. Res. 14 (1) (2019) 1–8.
[35] S.-H. Hwang, J.-K. Ku, Gingival Swelling and Erythematous with DBM Incorporated with rhBMP-2 after Large Postoperative Cystic Defect: a Case Report, 2020.
[36] I. Hartley, M. Zhadina, M.T. Collins, A.M. Boyce, Fibrous dysplasia of bone and McCune–Albright syndrome: a bench to bedside review, Calcif. Tissue Int. 104 (5) (2019) 517–529.
[37] W.H. Harris, Wear and periprosthetic osteolysis: the problem, Clin. Orthop. Relat. Res. 393 (2001) 66–70.
[38] T. Lange, A.F. Schilling, F. Peters, F. Haag, M.M. Morlock, J.M. Rueger, M. Amling, Proinflammatory and osteoclastogenic effects of beta-tricalciumphosphate and hydroxyapatite particles on human mononuclear cells in vitro, Biomaterials 30 (29) (2009) 5312–5318.
[39] D.A. Chistiakov, M.C. Killingsworth, V.A. Myasoedova, A.N. Orekhov, Y.V. Bobryshev, CD68/macrosialin: not just a histochemical marker, Lab. Invest. 97 (1) (2017) 4–13.
[40] F. Loi, L.A. Córdova, J. Pajarinen, T.-h. Lin, Z. Yao, S.B. Goodman, Inflammation, fracture and bone repair, Bone 86 (2016) 119–130.
[41] M.K. Chang, L.-J. Raggatt, K.A. Alexander, J.S. Kuliwaba, N.L. Fazzalari, K. Schroder, E.R. Maylin, V.M. Ripoll, D.A. Hume, A.R. Pettit, Osteal tissue macrophages are intercalated throughout human and mouse bone lining tissues and regulate osteoblast function in vitro and in vivo, J. Immunol. 181 (2) (2008) 1232–1244.
[42] L. Vi, G.S. Baht, H. Whetstone, A. Ng, Q. Wei, R. Poon, S. Mylvaganam, M. Grynpas, B.A. Alman, Macrophages promote osteoblastic differentiation in vivo: implications in fracture repair and bone homeostasis, J. Bone Miner. Res. 30 (6) (2015) 1090–1102.
[43] F. Zhang, E.A. Ayaub, B. Wang, E. Puchulu-Campanella, Y.H. Li, S.U. Hettiarachchi, S.D. Lindeman, Q. Luo, S. Rout, M. Srinivasarao, Reprogramming of profibrotic macrophages for treatment of bleomycin-induced pulmonary fibrosis, EMBO Mol. Med. 12 (8) (2020), e12034.
[44] E. Gruskin, B.A. Doll, F.W. Futrell, J.P. Schmitz, J.O. Hollinger, Demineralized bone matrix in bone repair: history and use, Adv. Drug Deliv. Rev. 64 (12) (2012) 1063–1077.